Cavarretta, I. *et al.* (2010). *Géotechnique* **60**, No. 6, 413–423 [**doi:** 10.1680/geot.2010.60.6.413]

# The influence of particle characteristics on the behaviour of coarse grained soils

I. CAVARRETTA*, M. COOP† and C. O'SULLIVAN†

**This paper describes an experimental study examining the influence of the mechanical and geometrical properties of the constituent grains on the overall material response of cohesionless granular materials. Glass ballotini were used as an analogue soil; their relatively simple geometry allowed the influence of particle shape and inter-particle friction to be examined independently. Techniques were developed to control the surface roughness of the ballotini to facilitate a parametric study. The particle shape was also varied by crushing the ballotini. At the micro-scale, the particle characterisation included accurate measurements of inter-particle friction, contact stiffness, particle surface roughness and particle shape. At the macro-scale the sensitivity of overall material response to changes in surface roughness and geometry was characterised using triaxial tests and oedometer tests on smooth spherical ballotini, roughened ballotini and crushed angular ballotini. Compression tests indicated that the initial load deformation response at particle–particle contact points is significantly softer than previously believed. Optical interferometry of particles after single particle–particle shearing tests confirmed that plastic strains occurred at the contact point, which were related to plastic yield. A Hertzian response was only seen at higher contact loads. A clear relationship between the inter-particle friction and the particle surface roughness was found. However, the macro-scale experiments indicated that while the material response may be slightly dependent on the surface roughness and friction, the influence of particle shape is very much more significant.**

**KEYWORDS: friction; shear strength**

**La présente communication décrit une étude expérimentale qui se penche sur l'influence des propriétés mécaniques et géométriques des grains constituants sur la réaction générale des matières dans des matériaux granulaires sans cohésion. On a utilisé des ballotines de verre comme sol analogique, leur géométrie relativement simple permettant d'examiner indépendamment l'influence de la forme des particules et de la friction interparticulaire. Des techniques ont été mises au point pour contrôler la rugosité de surfaces, afin de faciliter une étude paramétrique, et on a également varié la forme des particules par le broyage de ballotines. Au niveau de la micro-échelle, on a procédé à la caractérisation de la sensibilité de la réaction globale des matières aux variations de la rugosité de surface et de la géométrie par le biais de tests triaxiaux et avec consolidomètre sur ballotines sphériques lisses, ballotines rugueuses, et ballotines angulaires broyées. Des essais de compression ont indiqué que la réaction initiale aux déformations sous charge aux points de contact entre particules est sensiblement plus douce que celle des hypothèses initiales. De plus, l'interférométrie de particules à la suite d'essais de cisaillement individuelles entre particules a confirmé que des contraintes plastiques se produisent au point de contact, qui se rapportent à l'allongement plastique. On n'a relevé une réponse hertzienne qu'à des points de contact supérieurs. On a relevé un rapport évident entre la friction interparticulaire et la rugosité de surface. Toutefois, des expériences à macro-échelle ont indiqué que, même si la réaction des matières est légèrement tributaire de la rugosité de la surface et de la friction, l'influence de la forme des particules est beaucoup plus significative.**

## INTRODUCTION

As it is a particulate material, soil response is highly complex and the relationship between the nature of the individual particles and the overall material response remains poorly understood. Here the nature of a soil particle is defined as the combination of its geometry (roughness and shape) and its mechanical response (strength and stiffness). Over the past decade significant progress has been made; for example the relationship between particle strength and compression behaviour has been investigated in detail by McDowell & Bolton (1998) and Nakata *et al.* (1999), while the discrete element method (DEM) analyses of Thornton (2000) and others have indicated a stronger correlation between the macro-scale angle of shearing resistance and inter-particle friction than the experimental work of Skinner (1969). In the small strain region, Clayton & Heymann (2001) demonstrated that particle shape can have a significant impact on stiffness. The current study adds to this recent research by exploiting new technologies to quantify accurately particle shape and roughness, and by using custom-built apparatuses to measure particle contact stiffness and inter-particle friction. These particle scale, micro-mechanical measurements were coupled with conventional soil mechanics tests (oedometer and triaxial) to provide experimental data to relate the nature of the constituent particles with the macro-scale (overall) mechanical response of the soil. In contrast to earlier experimental micro-mechanical studies that have considered particle crushing and macro-scale yield, this work has focused on the behaviour of particles under the small loads that are often typical of engineering stress levels.

Tests were carried out on eight particle types, the details of which are given in Table 1. Glass ballotini were used as an analogue soil; tests on the as-supplied ballotini were compared with tests on roughened and crushed ballotini to explore the influence of roughness and shape on response. The roughness was increased either by rotational milling with a mixture of quartz sand and steel balls for 18–24 h or by etching using hydrofluoric acid (concentrations 1–40%) for immersion periods between 1 min and 3 h. Shape

Manuscript received 6 February 2009; revised manuscript accepted 23 October 2009.
Discussion on this paper closes on 1 November 2010, for further details see p. ii.
* Bristol University, formerly Imperial College London, UK.
†Geotechnics Section, Department of Civil and Environmental Engineering, Imperial College London, UK

**Table 1. Characteristics of the particles**

| Particle | Size range: mm $d_{min}$ – $d_{max}$ | Sphericity, $s$ | Roundness, $r$ | Circularity, CR | Regularity, $\rho$ | Roughness, $RMS_f$: μm | Inter-particle friction angle (°) dry | Inter-particle friction angle (°) wet | Young's modulus: MPa | Hardness: GPa |
|---|---|---|---|---|---|---|---|---|---|---|
| Small ballotini: as supplied | 1·0–1·4 | 0·98 | 0·97 | 1·00 | 0·96 | 0·1 | 9 | 6–15 | 70 000 | ≈1·5 (Kendall, 1969) |
| Large ballotini: as supplied | 2·4–3·0 | 0·95 | 0·97 | 1·00 | 0·97 | | 10 | 15 | | |
| Small ballotini: roughened-milled | 1·0–1·4 | 0·98 | 1·00 | 1·00 | 0·98 | 0·2–0·3 | 10 | 17 | | |
| Large ballotini: roughened-milled | 2·4–3·0 | – | – | – | – | | 15 | 22 | | |
| Small ballotini: roughened-etched | 1·0–1·4 | – | – | – | | 0·2–1·3 | 10 | 17 | | |
| Large ballotini: etched-milled | 2·4–3·0 | – | – | – | – | | – | – | | |
| Ballotini: Crushed | 1·0–1·4 | 0·3–0·9 | 0·1–0·7 | 0·6–0·9 | 0·2–0·7 | – | – | – | | |
| Leighton Buzzard sand A+B | 0·7–2·2 | 0·4–0·9 | 0·1–0·6 | 0·8 | 0·4–0·7 | 0·3 | 15–20 | | 70 000 | 9 (Grabco *et al.*, 2002) |

variation was achieved by crushing larger ballotini with a pestle and mortar; only the 1–1·4 mm fraction of this crushed material was then used in testing to match the size range of the smaller as-supplied ballotini.

## PARTICLE SHAPE DESCRIPTION

Table 1 gives the key characteristics of each particle. Sphericity, $s$, is defined as the ratio of the surface area of a sphere with the same volume as a particle to its actual surface area. Roundness, $r$, is calculated by drawing inscribed circles within each corner of a two-dimensional (2D) image of a particle and then taking the ratio of the average radius of those circles to the radius of the largest circle that may be inscribed within the particle outline. Circularity, CR, (essentially a 2D equivalent of $s$) equals $R_e^2$, where $R_e$ is the ratio of the perimeter of a circle with the same area as the 2D outline of a particle to its actual perimeter. Regularity, $\rho$, is the mean of $s$ and $r$; use of this single parameter to relate shape and mechanical properties was proposed by Cho *et al.* (2006). In Table 1, where there was no significant variability of a given shape parameter, it is reported as a single number, otherwise a range is given.

Krumbein & Sloss (1963) produced a reference chart that is commonly used for shape analysis. This chart is arranged as a matrix of 20 images of standard particle shapes where each row provides examples with the same $s$ and five different values of $r$. Users can quantify $s$ and $r$ for a given particle by visual comparison with the shapes in this chart. It is important to note that the 'sphericities' given in this chart were actually based on aspect ratio, AR. As described in detail by Cavarretta (2009), relationships between the shape descriptors used in the current study were established by digitising this chart and obtaining the CR and AR values for these standard shapes using Matlab and the Axiovision image analysis software (Zeiss, 2008). As illustrated in Fig. 1, for these images that are representative of a range of natural particle shapes, there are linear relationships between CR and $\rho$ and between AS and $s$.

The CR values given in Table 1 used $R_e$ values obtained from a Sympatec QicPic particle analyser. This apparatus scans particles falling under gravity with a laser, recording an outline of random orientation. The as-supplied ballotini were not perfectly spherical, but their regular shape meant that $s$ and $r$ could be calculated by assuming them to be ellipsoids and making manual measurements of their three principal diameters using a micrometer. For the crushed

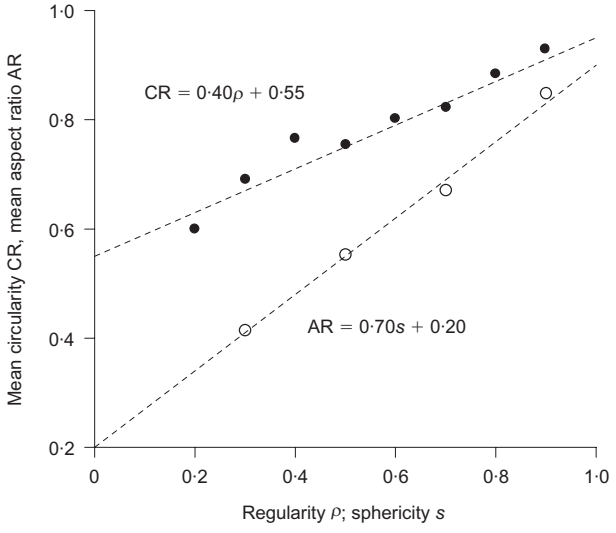


**Fig. 1. Correlations between shape descriptors**

ballotini the CR and AR values were measured using the QicPic, and $s$, $r$ and $\rho$ values were derived using the correlations given in Fig. 1. The shape parameters for representative crushed ballotini are presented along with their binary images captured with the QicPic in Fig. 2. The CR values obtained were validated using Matlab and the calculated $r$ and $s$ values were similar to those obtained using the Krumbein & Sloss chart. Validation of the AR values used images obtained from the QicPic and considered the ratio of the smallest and largest Feret diameters. While the $r$ and $s$ values were generally close to those obtained using the Krumbein & Sloss chart, for the most highly angular and convex crushed glass particles, the linear regression gave negative values for $r$, consequently a value of $r = 0{\cdot}1$ was set as a lower bound to the data. For the natural particles the values of $s$, $r$ and hence $\rho$ were obtained using the Krumbein & Sloss chart and confirmed using the QicPic and the correlations given in Fig. 1.

In this study the authors have chosen to quantify roughness directly using high-quality, objective measurements, rather than to use a fractal dimension type approach. The roughness measurements were made with a Fogale Nanotech optical interferometer. Roughness was quantified as the root mean square (RMS) deviation of the surface from its average level ($RMS_f$); the surface was automatically flattened by the processing software to remove the influence of shape on the calculated $RMS_f$ value. This flattening process involved discretising the surface in plan view into a grid of 28 μm squares and finding, for each square, the planar surface that best fitted the real three-dimensional (3D) surface. The roughness values were then calculated considering the difference between these planar surfaces and the measured surface. A parametric study considered grid spacings less than 28 μm and no noticeable change in the roughness was observed. A typical interferometer image for an etched ballotini is shown in Fig. 3. The range of roughnesses for the etched ballotini represents the minimum and maximum values for the various immersion times and concentrations of hydrofluoric acid.

Each shape and roughness parameter was determined with a sample of measurements large enough so that the average value obtained was not sensitive to additional measurements, the number required depending therefore on the variability of the particles. The QicPic apparatus makes automatic measurements for many thousands of particles while the manual measurements of the dimensions of the as supplied ballotini were made on around 120 particles. Where the Krumbein & Sloss chart was used to obtain shape parameters, around 30–40 particles were examined. For roughness, at least ten measurements were made for each particle type.

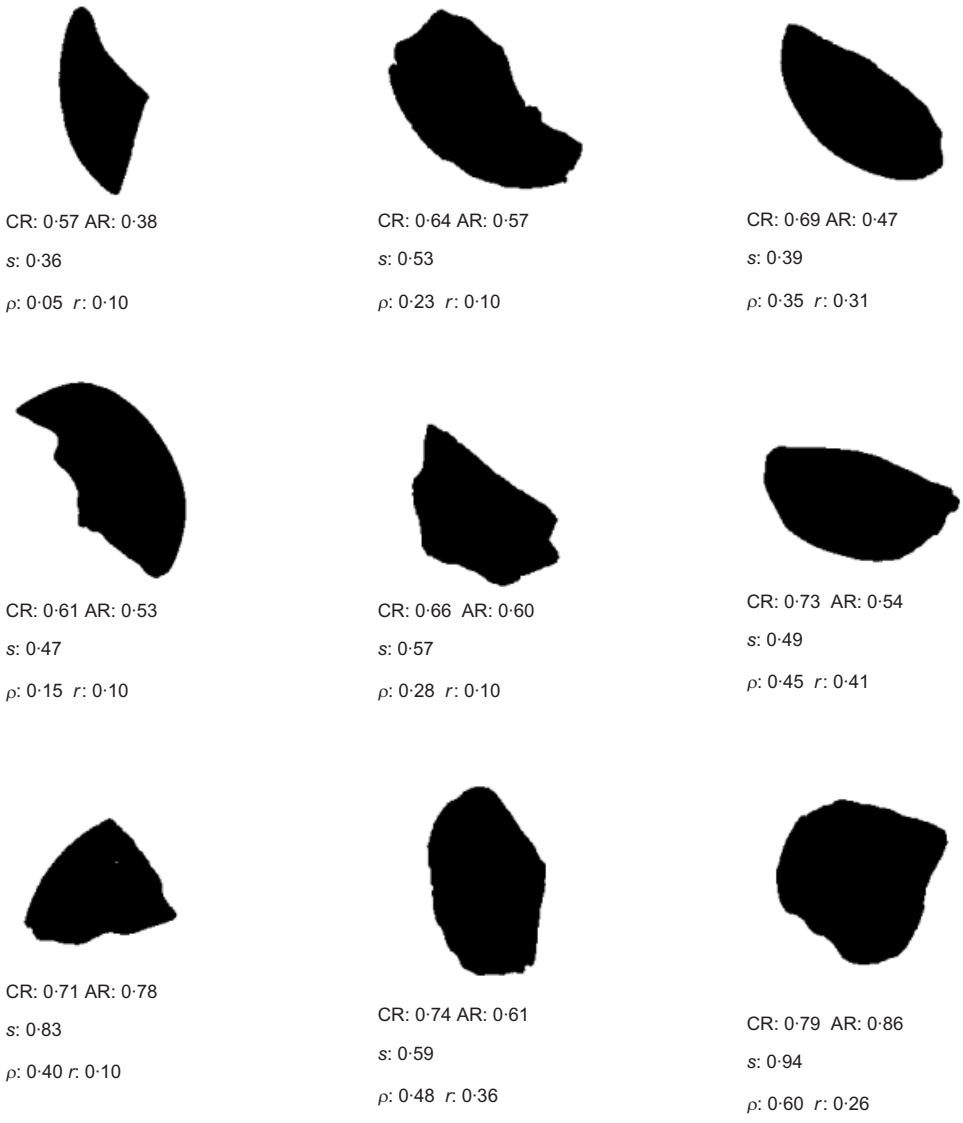


**Fig. 2. Binary images and shape parameters for representative crushed ballotini**

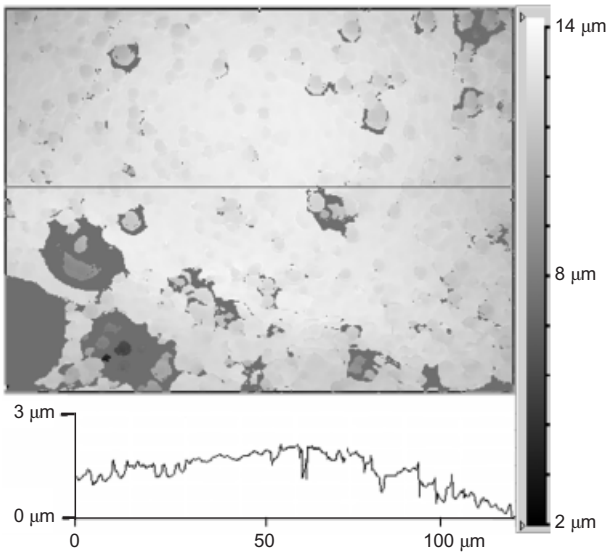


**Fig. 3. Interferometer image of an etched ballotini (60 min immersion at 2% concentration HF; $d_{mean} = 2{\cdot}49$ mm, $RMS_f = 0{\cdot}655\ \mu m$)**

## UNIAXIAL COMPRESSION TESTS

Compression tests were carried out on individual particles using the apparatus shown in Fig. 4 and three typical force–displacement ($N$–$\delta$) plots for the initial part of loading are given in Fig. 5. Initially the response is relatively soft and then there is a transition to a stiffer response. The displacement to this transition point increases with roughness. Fig. 5(a) gives a typical test where the response during unloading was also considered. It is clear after unloading that significant plastic deformation must have occurred during the earliest stage of loading. This observed plasticity could not have been the result of indentation of the loading platen as the loads are very small, and the hardness of the platen is around seven times that of the ballotini. Referring to Fig. 4, compliance of the apparatus has been minimised by excluding the load cell deformations from the displacements measured by the linear variable displacement transducers (LVDTs) and geometrical considerations exclude the possibility of particle rotation.

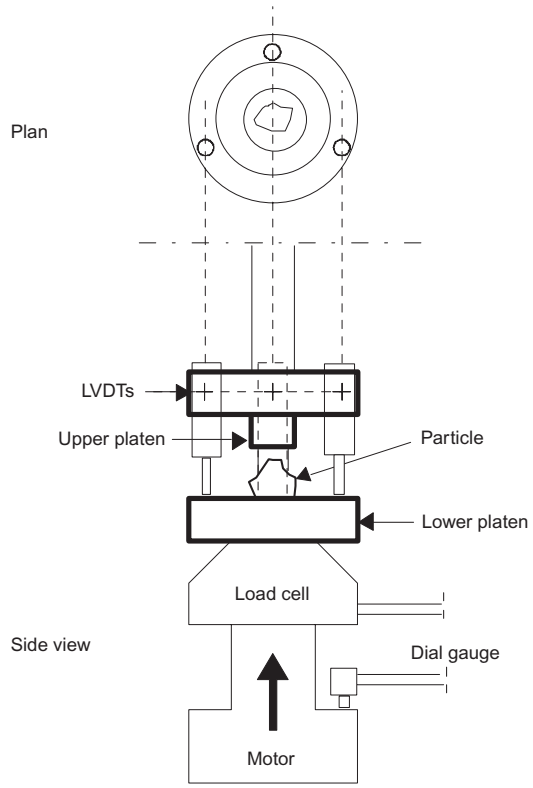


**Fig. 4. Particle compression apparatus**

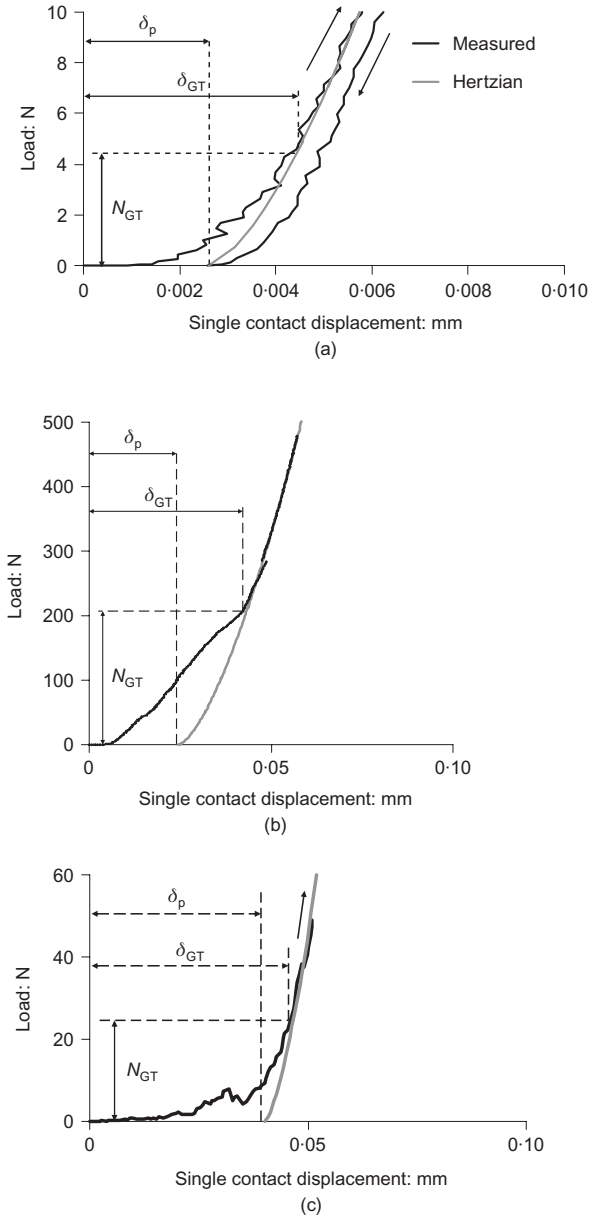


**Fig. 5. Typical compression test data at small displacements: (a) smaller ballotini in as-supplied state ($d_{mean} = 1{\cdot}24$ mm, $RMS_f = 0{\cdot}080$ μm); (b) etched larger ballotini ($d_{mean} = 2{\cdot}49$ mm, $RMS_f = 0{\cdot}655$ μm); (c) Leighton Buzzard sand, type A ($d_{mean} = 1{\cdot}67$ mm, $s = 0{\cdot}6$, $r = 0{\cdot}8$, $RMS_f = 0{\cdot}3$ μm).**

For an elastic response, a prediction of the $N$–$\delta$ curve may be made on the basis of Hertzian theory, which is often used in DEM contact models

$$N = \frac{4}{3} R^{0{\cdot}5} E^* \delta^{3/2} \tag{1}$$

where $R$ is given by $1/R = 1/R_1 + 1/R_2$, and $R_1$ and $R_2$ are the radii of the contacting surfaces. The relative Young's modulus, $E^*$, is given by

$$\frac{1}{E^*} = \frac{1 - \nu_1^2}{E_1} + \frac{1 - \nu_2^2}{E_2} \tag{2}$$

where $\nu$ is the Poisson's ratio and the subscripts 1 and 2 again refer to the two surfaces (Johnson, 1985). For the as-supplied ballotini test in Fig. 5(a) a Hertzian curve was fitted to the stiffer region of the load–displacement curve. If it is assumed that $\nu_1 = \upsilon_2 = 0{\cdot}2$, and the Young's modulus of the steel platen is 200 GPa, by applying equation (1) the Young's modulus for the glass ballotini was calculated to be 70 GPa. This value is very close to the manufacturer's value of 77 GPa. It therefore appears that while at larger displacements there is elastic behaviour, the initial contact displacements are plastic in nature and are likely to result from damage to asperities. Kendall (1969) observed similar pre-Hertzian behaviour in glass, and Kendall's findings informed the development of the JKR contact model (Johnson *et al.*, 1971). The JKR model is generally applied to contacts between soft solids such as rubber. Greenwood & Tripp (1967) also measured a similar response for rough hard materials, and they showed that a Hertzian relationship would be followed only after a threshold load, $N_{GT}$, had been reached at a displacement $\delta_{GT}$

$$N_{GT} \cong 100\,(\mathrm{RMS_f})\;E^*[2R\;(\mathrm{RMS_f})]^{0{\cdot}5} \tag{3}$$

$N_{GT}$ values were calculated using the measured roughnesses and values of $E^*$ evaluated using the curve-fitting procedure described above. As illustrated in Fig. 6 these predicted values ($N_{GT}^{pred}$) were very close to the observed force at the onset of Hertzian response ($N_{GT}^{meas}$). Each data point in Fig. 6 represents an individual test. While additional data points would introduce some scatter, the data presented clearly indicate good agreement between the experiments and theory. The 'effort index' used in Fig. 6 represents the extent of the etching as the product of the acid concentration and the time of immersion, normalised by the minimum immersion time of 1 min.

Considering the response for displacements less than $\delta_{GT}$, initially full plasticity (yielding) occurs, up to a displacement $\delta_p$. Then, there is a stage of combined elastic and plastic deformation before $\delta_{GT}$ is reached and the response becomes Hertzian. The observed response can be explained by realising that the initial contact area between two spherical particles is zero (whether rough or smooth). Consequently at very small displacements the contact stresses easily reach the yield pressure of the material, $p_y$. As shown schematically in Fig. 7, the initial part of the $N$–$\delta$ curve will therefore be controlled by yielding of the material at a constant average contact pressure, $p_{mean}$, that equals $p_y$, and the displacement must be sufficiently large that the product of the contact area and $p_{mean}$ equals $N$. There is a specific displacement, $\delta_p$, beyond which the contact area becomes large enough to have some Hertzian elastic behaviour. At this point it can be assumed that the plastic flow of the deforming asperities will have practically filled the troughs between asperities, so that the central region of the contact is almost contiguous. The contact topology and the non-uniform stress conditions mean that after this point the central region of the contact is yielding, with the material at the edge of the contact responding elastically. This mixed elastic and plastic response continues until the displacement $\delta_{GT}$ is reached and fully Hertzian response is observed.

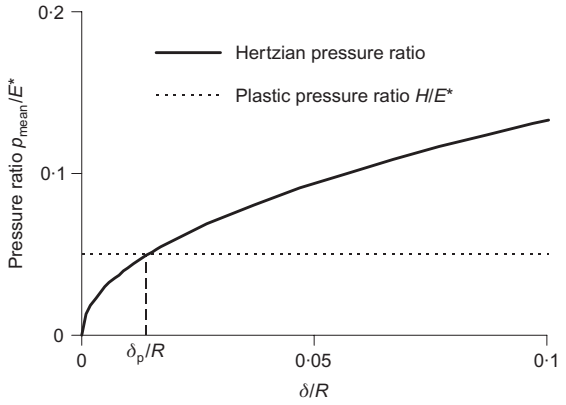


**Fig. 7. Schematic relationship between mean contact pressure and displacement**

The value of $\delta_p$ can be theoretically estimated by considering that for imperfect surfaces with non-zero roughness the real contact area during the plastic deformation of the asperities, $A_r$, will be created by flattening of the asperities. This total contact area, which may not be continuous, is expressed as a proportion, $\alpha$, of the apparent area of contact, $A_a$. For glass, typical $\alpha$ values are as much as 0·8–1 (Marsh, 1964), indicating that the plastic flow of the glass around the deforming asperities gives an $A_r$ almost equal to $A_a$. During plastic deformation of the asperities $p_y \approx 1{\cdot}2\alpha H$ (Childs, 1977). The mean pressure is given by $p_{mean} = A_r p_y / A_a$. The value of $\delta_p$ can then be calculated by equating the Hertzian pressure with $p_{mean}$ ($= 0{\cdot}8 \times 1{\cdot}2H \approx H$), so that

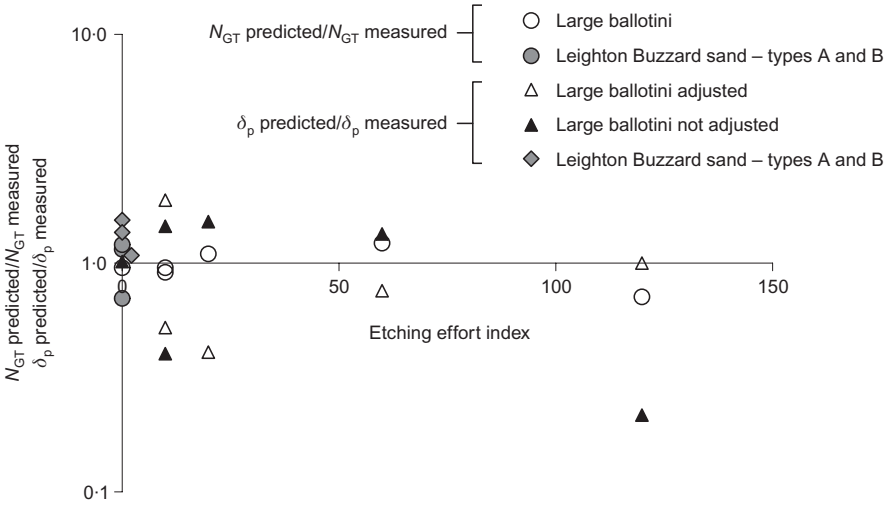


**Fig. 6. Comparisons between measured and predicted threshold loads, $N_{GT}$ and initial plastic displacements, $\delta_p$**

$$\delta_p = \frac{9R\pi^2}{16}\left(\frac{H}{E^*}\right)^2 \quad (4)$$

The predicted values of $\delta_p$ are again compared with the measured values on Fig. 6. The agreement is good for the as-supplied ballotini, as indicated for the data point for the 'non-adjusted etched ballotini' at zero effort index. However, as the etching also increases the hardness (Denisenko *et al.*, 1976), the ratio $\delta_p{}^{meas}/\delta_p{}^{pred}$ reduces as the etching increases. A correction was therefore made, assuming that the hardness increased linearly with the etching effort, and a gradient of 22 MPa per unit effort index gave the best fit to the data.

A typical $N$–$\delta$ curve for a natural particle of Leighton Buzzard sand (type A) is shown in Fig. 5(c). The value of $RMS_f$ of 0·3 μm is an average value for this sand. For a natural particle with an irregular shape, it is not evident which radius should be chosen to calculate the equivalent radius, $R$. Clearly $R$ should be related to the roundness of the particle rather than to its size, and so a mean radius of the corners has been used calculated from

$$\frac{1}{R} = \frac{2}{r\, d_{imax}} \quad (5)$$

where $d_{imax}$ is the diameter of the largest inscribed circle within the particle outline. The comparison between predicted and measured values of $\delta_p$ and $N_{GT}$ based on this assumption and given in Fig. 6 is again reasonably good. Referring to Fig. 6, the observed scatter in the data reflects the additional sensitivity of the response to the precise nature of the asperity topology at the contact point; the extent of the local variations in the asperity geometry can be appreciated by reference to Fig. 3.

Assuming a power-law response when $\delta < \delta_p$, and zero stiffness at $\delta = 0$, the expression for the loading curve ($N_p$) as a function of $\delta$ is given by

$$N_p = N_{GT}\delta_{GT}^{-b}\delta^b \quad (6)$$

where $b$ is a dimensionless constant given by

$$b = 2E^*\left[R\left(\delta_{GT} - \delta_p\right)\right]^{0.5}\delta_{GT}N_{GT}^{-1} \quad (7)$$

The plastic stiffness $K_{np}$, is the first derivative of $N_p$ with respect to $\delta$ and it equals the Hertzian stiffness value at $\delta = \delta_{GT}$.

Barreto Gonzalez (2009) gives data for a DEM simulation of an assembly of spheres whose particle size distribution matched that of the small ballotini and which was subject to isotropic compression to 400 kPa. The results indicated that 80% of the contact forces were less than 0·1N and only within the strong force chains were values up to 1·3N seen. These values of contact force are much smaller than typical $N_{GT}$ values observed (about 4 N). Therefore, for most engineering applications the contact behaviour between particles of this size will certainly be in the range of plastic response, well below $\delta_p$. Particle rearrangement during loading will also create fresh contacts with new asperities to deform plastically.

## INTER-PARTICLE FRICTION TESTS

Previous studies of the friction between particles have tended to concentrate on how the parent material affects the behaviour, either by using apparatuses in which two particles of the same material are sheared one over the other (Skinner, 1969; Barton, 1972) or by rubbing a single particle against a flat surface of similar mineralogy (e.g. Horne & Deere, 1962, Dickey, 1966). Previous granular mechanics studies have not considered the influence of the internal properties of the material, in particular the Young's modulus and hardness, and comparisons between the various studies are therefore complicated by the interaction of the various properties that might affect the friction measured. The approach adopted here was to change the roughness of the glass ballotini, while all other properties were unchanged. From compression tests it was realised that etching changed the surface hardness and the Young's modulus. The interferometer images (Fig. 3) also revealed that, although the overall sphericity was not greatly influenced, the process created some craters on the particle surface. These induced features were at a scale lying between the scales of roughness and overall form, and can be considered to have affected the texture or waviness of the particle surface. A milling procedure was then developed to change the ballotini roughness without altering other properties. It was also found that it gave a more uniform and repeatable roughness.

Frictional experiments on alkaline glass ballotini have proven problematic in the past because of the scatter of results. Barton (1972) highlighted the importance of the cleanliness of the surface of a dry ballotini in order to avoid strong effects of surface chemistry and lubricating contaminated layers. He claimed that the scatter of data from Skinner (1969) resulted from the use of contaminated particles. Barton showed also that water acts as an anti-contaminant and that the higher the roughness the smaller the effects of surface chemistry.

A new inter-particle friction apparatus, designed and built for the current study, is illustrated in Fig. 8. During each test

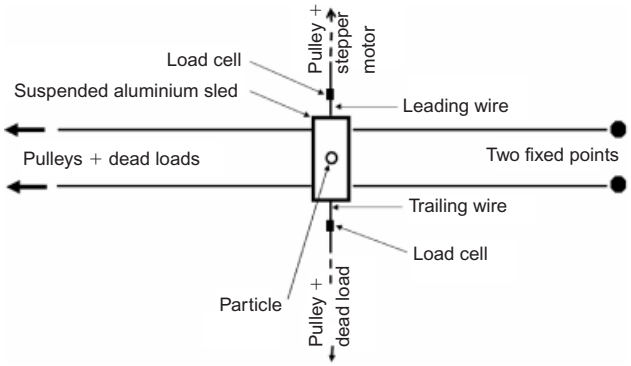


(a)

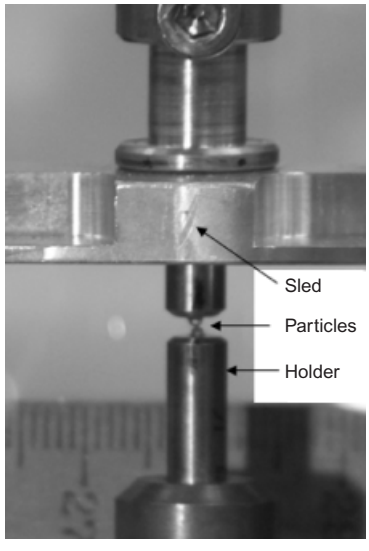


(b)

**Fig. 8. The inter-particle friction apparatus: (a) schematic plan; (b) side view**

one particle is sheared over the top of a second stationary particle. It was designed to ensure that the moving particle would be constrained to travel in a straight line and would not be permitted to skate around the side of the lower one. This is achieved by gluing the two particles into holders. The upper holder is held in a sled constrained to travel in a straight line by two metal wires running orthogonal to the direction of travel. These wires are tensioned with dead weights hanging over pulleys located 35 cm from the sled, a distance sufficient to minimise any resistance to movement. In the direction of travel the sled is pulled by a leading wire attached to a stepping motor. A trailing wire attached to the rear of the sled is held taught with a dead weight acting over a pulley. The horizontal force, $F_h$, is measured by taking the difference between the readings of load cells in the leading and trailing wires. A small chamber can be positioned around the two particles and filled with de-ionised water to measure the change of friction on immersion. Two LVDTs measured the vertical and horizontal displacements of the upper particle. The laboratory temperature and humidity were also data-logged.

Two versions of the apparatus were built. Initially it was designed for a minimum vertical load of about 2·3 N, with a load cell accuracy of about ±0·1 N, giving values of inter-particle friction angle, $\phi_\mu$, with a precision of about ±2°. In the refined apparatus, the minimum load is 0·9 N, the accuracy of the load cells is ±0·02 N and the friction angle measurement accuracy is ±1°. A speed of shearing in the range 140–200 μm/h was used throughout. The resistance provided by the apparatus to horizontal and vertical movements was calibrated; checks based on statics gave results within ±0·01 N of the calibrations. Great care was taken to avoid contamination of the shearing surfaces of the particles with glue or with grease from finger contact, and each surface was also cleaned with butanone prior to shearing to remove dust and any chemical contamination.

When one particle is sheared over another, the measured horizontal force ($F_h$) will only give the correct inter-particle friction when the apex of the lower particle is reached, and no dilative or compressive component of displacement affects $F_h$. Referring to Fig. 9, when the contact normal is inclined at $\alpha$ to the vertical a consideration of the forces acting on the particle gives the following

$$F_v = N\cos\alpha - N\mu\sin\alpha \quad (8)$$

$$F_h = N\sin\alpha + N\mu\cos\alpha \quad (9)$$

The inter-particle coefficient of friction, $\mu$ ($= \tan\phi_\mu$) and the normal contact force, $N$ are found by solving these simultaneous equations. At any point the angle $\alpha$ can be read as the tangent to the vertical displacement–horizontal displacement curve. Shearing can only take place under a horizontal force alone if $\alpha < 90 - \phi_\mu$.

Comparisons of interferometer data for the same surface before and after shearing provide evidence that plastic damage occurred. The example shown in Fig. 10 considers shearing of two of the smaller ballotini using a vertical force of 2·3 N which is less than half the $N_{GT}^{pred}$ value for these particles (4·5 N). The sections illustrated have been taken through the particle apex where contact between the particles occurred. There is clear evidence of damage, with increased roughness along the section and some ploughing just after the apex was passed.

Typical shearing data are shown in Fig. 11. While there is some variation in the calculated $\phi_\mu$ during shearing, a value of 7·7° may be estimated around the apex, where the dilational component is zero and so the data may be more accurate. Measured $\phi_\mu$ values for the small ballotini in a dry state are given in Fig. 12. The roughness variation was achieved using milling and although there is considerable scatter at higher roughnesses, there is a clear increase of $\phi_\mu$ with $RMS_f$ (the values given are the mean $RMS_f$ values for the two ballotini). In each case, following the first shear test, the top ballotini was rotated through 90° and the test repeated, to examine the effect of any plastic damage caused by the first shearing. For the as-supplied, smooth ballotini, the data show a small increase of $\phi_\mu$, but for the roughened ballotini the $\phi_\mu$ generally decreased a little. The differences between first and second shearing of the roughened ballotini were generally within the ±20% error bars shown around the data point for the first shearing. The wide scatter of $\phi_\mu$ values is therefore a true reflection of the behaviour of the particles created.

A summary of the $\phi_\mu$ values for the various materials considered in this study is given in Table 1. The refined

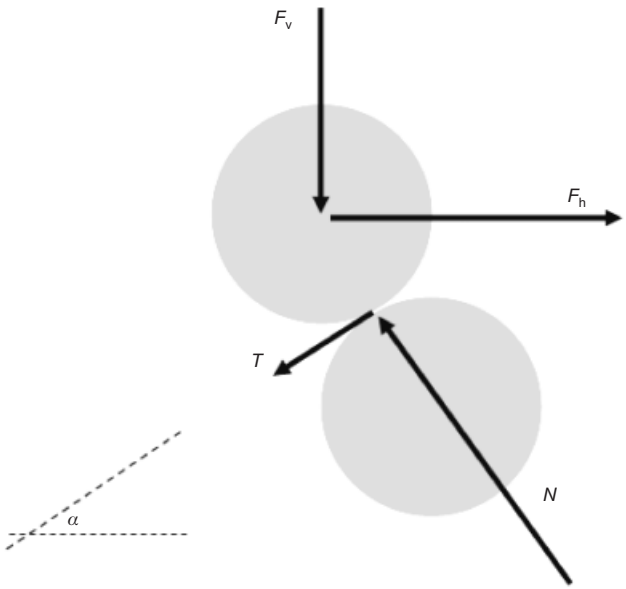


**Fig. 9. Forces acting on the contact between two particles during shearing**

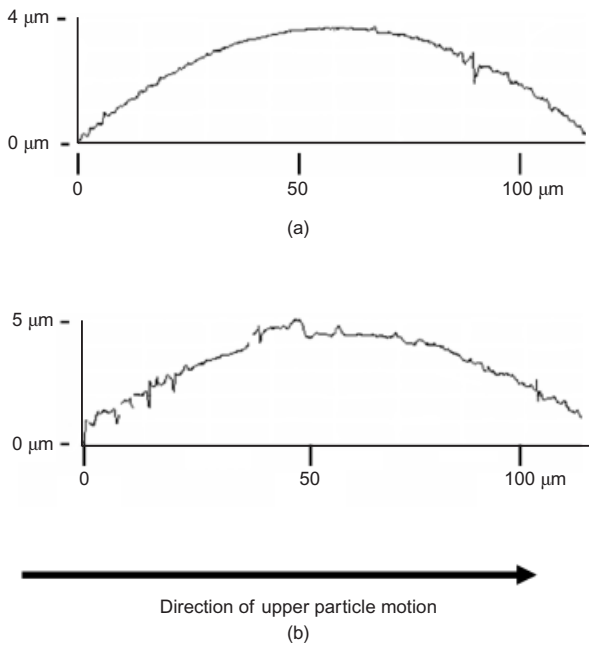


**Fig. 10. Interferometer sections through surface of upper particle before and after shearing two smaller ballotini: (a) before; (b) after**

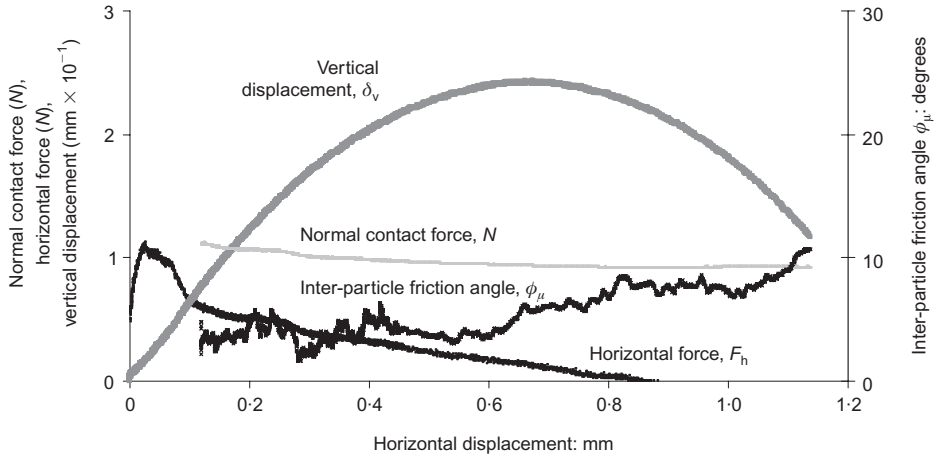


**Fig. 11. Typical results from a friction test on smaller dry ballotini ($d_{mean} = 1{\cdot}06$ mm)**

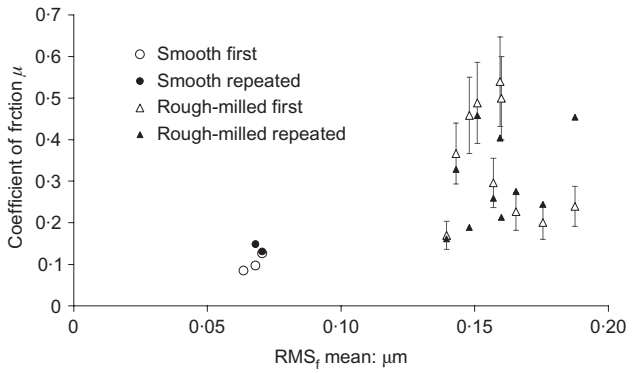


**Fig. 12. Measured inter-particle friction coefficients for the small dry ballotini**

apparatus was used to generate the data for the small ballotini, and the original apparatus was used in all other cases. While only those tests with a second shearing are considered in Fig. 12, a total of 20 tests were completed on the small, dry, as-supplied ballotini giving a mean $\mu = 0{\cdot}16$ ($\phi_\mu = 9{\cdot}4°$) with a standard deviation of 7·3% (i.e. about 4°). However, if the relative humidity of the laboratory rose above 45%, then there was a significant effect on the data, with a mean $\mu$ of 0·27 ($\phi_\mu = 15{\cdot}1°$) and standard deviation of 20·1%, for the nine tests carried out at higher humidities. This threshold relative humidity is in agreement with the value of 40% found by Horne & Deere (1962) for shearing a glass sphere against a glass plate. The lower variability among the eight saturated test measurements (standard deviation of only 2%) corresponded with the findings of Barton (1972). There was no consistent difference between the wet and dry states for the small as-supplied ballotini, although more stick–slip type response was observed in the dry tests. It is not evident that the value of $\mu$ should be similar for the saturated and dry tests, as the contact of submerged surfaces can involve complex interactions between water menisci and the surfaces, the effects of the water on any contaminated layers between the particles and any chemical effects between surface water and that absorbed into the surface. However, in the case of the small as-supplied ballotini the value of $\mu$ is similar for the dry and saturated test conditions, in contrast to the results of Skinner (1969). For the other particles tested small increases in friction were seen upon immersion.

## MACROSCOPIC TESTS

The influence of these particle scale measurements on the overall material response was explored in a series of conventional soil mechanics tests. While previous studies have considered the overall response of ballotini specimens, it was important here to test the same materials as had been considered in particle scale characterisation, rather than relying on previously published data. Oedometer samples of the ballotini were made by gently air pluviating them into a 38 mm diameter oedometer ring from a funnel, then vibrating the sample to increase its density if necessary. Most of the tests were conducted dry, and typical data, shown in Fig. 13, resemble the compression curves of sands, in which a distinct yield indicates the onset of significant particle breakage (Coop & Lee, 1993; Bolton *et al.*, 2008). On unloading the behaviour is very stiff with a large permanent strain that results from the particle breakage.

The clearest differences between the various materials are those arising from the influence of particle shape, the spherical as-supplied ballotini having yield stresses and a normal compression line (NCL) at higher stress levels than the angular crushed ballotini. One test on a saturated sample of the crushed ballotini confirms that the presence of water

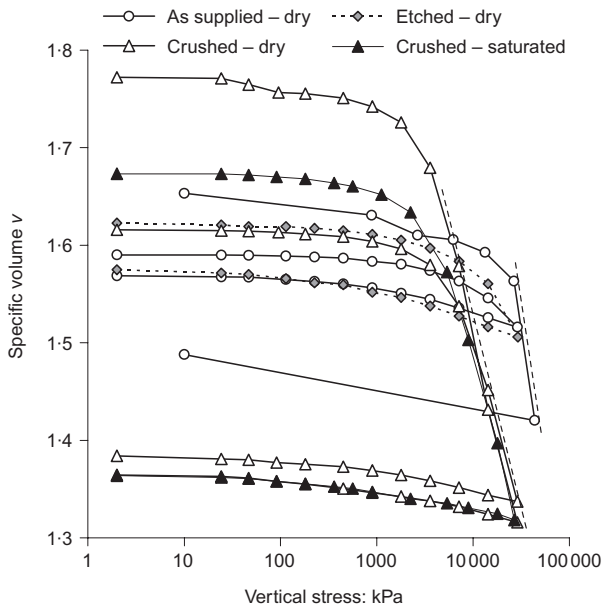


**Fig. 13. Oedometer test data for the ballotini**

has no effect on the compression behaviour. The NCL of the spherical ballotini is steeper than that of the angular, and the convergence of the two may reflect a reduction of the initial differences in particle shape as crushing continues. The differences of initial shape also influence the range of initial densities that can be created, with a much wider range for the crushed than for the spherical particles.

The effects of particle roughness are less evident, but a difference can be seen for tests that do not pass yield. Two tests were conducted on the spherical ballotini with similar initial specific volumes of around 1·6, one on an as-supplied ballotini and one on etched ballotini (for 1 h at 10% concentration, with $RMS_f = 0{\cdot}9–1{\cdot}2$ μm). Both were loaded to 3 MPa vertical stress, which is prior to the major yield, but the plastic strain on unloading the roughened ballotini is significantly larger. Tests were also carried out on the angular ballotini that were etched, but in this case the tests were taken past yield, and no difference could be seen in their behaviour.

The triaxial tests were carried out using the same ballotini, on samples of 38 mm diameter and 76 mm length. In this case the roughened ballotini had been milled for 18–24 h. Attempts were made to conduct the tests dry, but the volumetric strains that were derived from the local axial and radial strain transducers attached to the specimen were not sufficiently accurate at high strains to be able to identify the critical state volume with any certainty. The tests discussed here were therefore carried out saturated, with conventional volume change measurements made with a volume gauge.

From the stress–strain data in Fig. 14 it can be seen that each sample tends towards a critical state at the end of shearing; while the final stress ratios were fairly constant, for most tests there was still a slight continuing dilation despite the large strain levels reached. The end of test states in Fig. 15(a) clearly show the effect of particle shape on $M$ (or $\phi'_{cs}$). At higher stress levels it is not clear that the particle roughness has any effect on $M$, although at the lowest confining stress of 50 kPa, the data in Fig. 14 seem

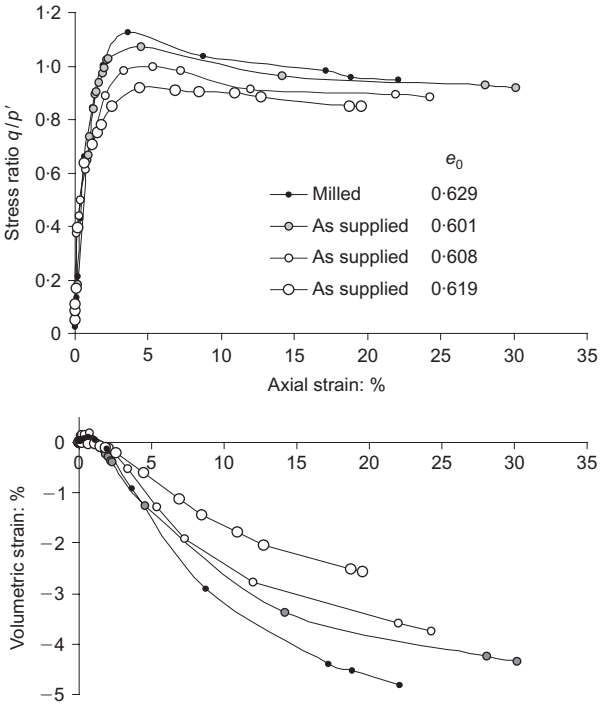


**Fig. 14. Stress–strain data for drained triaxial compression at 50 kPa confining stress**

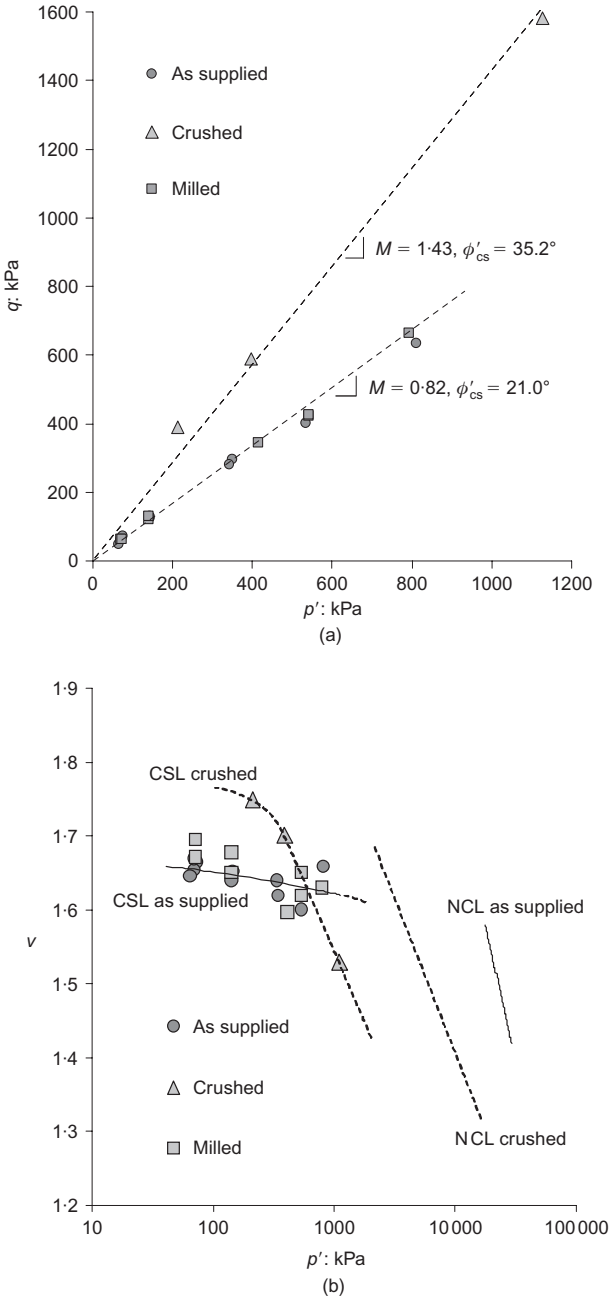


**Fig. 15. End of test states: (a) $q$–$p'$ plane; (b) $v$–ln$p'$ plane**

to show a higher $M$ for the roughened ballotini. It is possible that at higher stress levels the particle asperities become flattened and the effect of the initial roughness is lost.

In the $v$–ln$p'$ plane the data define critical state lines (CSL) that are initially curved, as they would be for sands. The data are a little scattered, because there was some difficulty in measuring the void ratios accurately, but for the crushed ballotini the CSL seems to become straight and parallel to the one-dimensional NCL at higher stress levels, but for the as-supplied ballotini only the flatter part of the CSL has been defined at the confining pressures of up to 600 kPa used for these tests. There is no significant effect arising from the particle roughness. The values of $p'$ for the one-dimensional NCLs have been estimated by using a $k_0$ of 0·51 that was measured by Barreto Gonzalez (2009) for the as-supplied ballotini, and a value of 0·42 for the crushed ballotini, which was estimated from $1 - \sin\phi'$.

## CONCLUSIONS

The increased use of DEM in geomechanics research, the limited available experimental data on inter-particle friction values and the discrepancy between the numerical and experimental findings, indicated a need to re-examine experimentally the relationship between inter-particle friction and overall material response. While prior research has considered the influence of gross yield (i.e. breakage) on soil response, the initial, pre-failure plasticity at particle contacts has received little experimental analysis in the geomechanics literature.

The laser scanning particle analyser and optical interferometer were found to give quick and convenient quantifications of particle shape and roughness, although an indirect method was developed to derive roundness, because it was not measured by the laser scanner.

At the micro-level, the particle compression tests revealed an initial response that was dominated by plasticity. The threshold force at which Hertzian behaviour takes over is dependent on topographical features of the particle (size, roundness and roughness) and the elastic bulk properties (Young's modulus). The initial plastic displacement depends on the same topographical and bulk features, but also depends on the surface hardness. A new formula for the normal contact stiffness for the pre-Hertzian response has been proposed, which may be of use in DEM simulations.

The inter-particle friction was measured by means of a new apparatus. While a clear relationship was found between inter-particle friction and roughness, the results were not always consistent with previous studies on the effect of complete immersion in water; while the relative humidity of the laboratory was found to be important.

In the macro-scale tests the influence of particle shape was much more noticeable than the influence of surface roughness (and hence inter-particle friction). In the oedometer apparatus, the more angular particles exhibited greater plasticity in their response, that is the decrease in specific volume during the load–unload cycle experienced in each test was greater for the angular particles than for the spherical particles. While the roughness of the particles did affect the compression behaviour pre-yield, the influence of shape was significantly more marked. The response observed in the triaxial tests was also much more sensitive to the particle shape in comparison with the surface roughness. Accepting, from the single particle tests, that the surface friction could be controlled by changing the surface roughness, it then could not be concluded that there was an increase in the overall shearing resistance of the material as the inter-particle friction increased. A possible explanation for the observed lack of sensitivity to friction is that the range of roughness values considered was too small, however, it is more likely that the stress levels were too high for the increase in inter-particle friction to be retained during initial, isotropic compression of the sample. The response in the single particle compression tests indicated that even in the absence of inter-particle shearing, the contact normal forces can crush the asperities and smooth the surface. Within the material there will be a significant variation in the contact normal forces, however, DEM simulations (e.g. Thornton, 2000) have demonstrated that the overall response is dominated by those particles that participate in the strong force chains. The contact forces between particles along the strong force chains are likely to be high enough to remove the roughening effect. The accurate measurement of the load–deformation behaviour during the single particle compression tests, coupled with characterisation of the surface roughness therefore provides an explanation for the discrepancy between the findings of Skinner (1969) and the reported results of many DEM analysts. Confirmation of this proposed mechanism requires further laboratory experiments involving accurate measurements of small strain stiffness (which was beyond the scope of the current study) as well as the development of a new type of DEM contact model. This new contact model should capture the destruction of asperities and resulting reduction in frictional resistance as a function of the normal component of the contact force. Then the yield parameter describing interaction in the contact tangential direction will be a function of the load history in the contact normal direction. Further data are required to inform the development of this model. It is also important to recognise that the results presented here are for (alkaline) ballotini, the response observed may be sensitive to the material hardness and further tests are required prior to extrapolation to sands.

## ACKNOWLEDGEMENTS

The authors would like to express their thanks to the technical staff of Imperial College for their input to the design of the compression and shear test apparatus. They are also grateful to Mr K. S. Chan, Ms Y. H. Wong, Ms M. W. Kwan and Ms M. Wu who carried out some of the oedometer and triaxial tests.

## REFERENCES

Barreto Gonzalez, D. (2009). *Numerical and experimental investigation into the behaviour of granular materials under generalized stress states*. PhD thesis, Department of Civil and Environmental Engineering, Imperial College London.

Barton, R. R. (1972). *A study of the angle of inter-particle friction of sands with respect to its influence on the mass strength*. MSc thesis. The Victoria University of Manchester, Manchester.

Bolton, M. D., Nakata, Y. & Cheng, Y. P. (2008). Micro- and macro-mechanical behaviour of DEM crushable materials. *Géotechnique* **58**, No. 6, 471–480, **doi**: 10.1680/geot.2008.58.6.471.

Cavarretta, I. (2009). *The influence of particle characteristics on the engineering behaviour of granular materials*, PhD thesis, Department of Civil and Environmental Engineering, Imperial College London.

Childs, T. H. C. (1977). The persistance of roughness between surfaces in static contact. *Proc. R. Soc. Lond. Ser. A, Mathl Phys. Sci*. **353**, No. 1672, 35–53.

Cho, G. C., Dodds, J. & Santamarina, J. C. (2006). Particle shape effects on packing density, stiffness, and strength: natural and crushed sands. *J. Geotech. Environ. Engng ASCE* **132**, No. 5, 591–602.

Clayton, C. R. I. & Heymann, G. (2001). Stiffness of geomaterials at very small strains. *Géotechnique* **51**, No. 3, 245–255, **doi**: 10.1680/geot.2001.51.3.245.

Coop, M. R. & Lee, I. K. (1993). The behaviour of granular solis at elevated stresses. In *Predictive soil mechanics. Proceedings of the Worth memorial symposium* (eds G. T. Houlsby and A. N. Schofield), pp. 186–198. London: Thomas Telford.

Denisenko, O. N., Shcheglova, O. V. & Sobolev, E. V. (1976). Influence of etching glass in hydrofluoric acid upon the hardening of the glass by low-temperature ion exchange. *State Scientific-Res. Inst. Glass*, **33**, No. 2, 13–14.

Dickey, J. W. (1966). *Frictional characteristics of quartz*. SB thesis, M.I.Y., Cambridge, MA.

Grabco, D., Palistrant, M., Shikimaka, R., Zhitaru, R., Rahvalov, V. & Zugravescu, D. (2002). Hardness and brittleness of rocks studied by microindentation method in combination with the registration of acoustic emission signals. *Proc. 8th Eur. Conf. Non- Destructive Testing, Barcelona*, CD-ROM.

Greenwood, J. A. & Tripp, J. H. (1967). The elastic contact of rough spheres. *Trans. ASME. J. Appl. Mech*. **34**, No. 1, 153–159.

Horne, H. M. & Deere, D. U. (1962). Frictional characteristics of minerals. *Géotechnique* **12**, No. 4, 319–335, **doi**: 10.1680/geot.1962.12.4.319.

Johnson, K., Kendall, K. & Roberts, A. (1971). Surface energy and the contact of elastic solids. *Proc. R. Soc. Lond. Ser. A, Mathl Phys. Sci*. **324**, No. 1558, 301–313.

Johnson, K. L. (1985). *Contact mechanics*. Cambridge: Cambridge University Press.

Kendall, K. (1969). *The stiffness of surfaces in static and sliding contact*. PhD thesis, Engineering Department, University of Cambridge, UK.

Krumbein, W. C. & Sloss, L. L. (1963). *Stratigraphy and sedimentation*. San Francisco: W. H. Freeman and Company.

Marsh, D. (1964). Plastic flow in glass. *Proc. R. Soc. Lond. Ser. A, Mathl Phys. Sci*. **279**, No. 1378, 420–435.

McDowell, G. R. & Bolton, M. D. (1998). On the micro mechanics of crushable aggregates. *Géotechnique* **48**, No. 5, 667–669, **doi**: 10.1680/geot.1998.48.5.667.

Nakata, Y., Hyde, A. F. L., Hyodo, M. & Murata, H. (1999). A probabilistic approach to sand particle crushing in the triaxial test. *Géotechnique* **49**, No. 5, 567–583, **doi**: 10.1680/geot.1999.49.5.567.

Skinner, A. E. (1969). A note on the influence of interparticulate friction on the shearing strength of a random assembly of spherical particles. *Géotechnique* **19**, No. 1, 150–157, **doi**: 10.1680/geot.1969.19.1.150.

Thornton, C. (2000). Numerical simulations of deviatoric shear deformation of granular media. *Géotechnique* **50**, No. 1, 43–53, **doi**: 10.1680/geot.2000.50.1.43.

Zeiss (2008). AxioVision Release 4.7.2 (Software). Carl Zeiss MicroImaging GmbH, Munich, Germany.